Chalcogenide Letters Vol. 12, No. 1, January 2015, p. 11 - 23

ELECTROCHEMICAL STUDIES OF PVP-CAPPED PbS THIN FILM DEPOSITED BY POLYMER-ASSISTED CHEMICAL BATH DEPOSITION (PACBD)

C. G. EZEMA[a,b], S. U. OFFIAH[a,c], A. C. NWANYA[a,c], P. O. UKOHA[b], B. E. EZEMA[b], M. MAAZA [d,e], F. I. EZEMA[c,d,e*]

[a]*National Centre for Energy Research & Development, University of Nigeria, Nsukka (UNN), Enugu State, Nigeria.*

[b]*Department of Pure and Industrial Chemistry, UNN, Nsukka, Enugu State, Nigeria.*

[c]*Department of Physics and Astronomy, UNN, Nsukka, Enugu State, Nigeria.*

[d]*Nanosciences African Network (NANOAFNET), iThemba LABS-National Research foundation, 1 Old Faure road, Somerset West, Western Cape Province, South Africa.*

[e]*UNESCO-UNISA Africa Chair in Nanosciences/Nanotechnology, College of Graduate Studies, University of South Africa (UNISA), Muckleneuk ridge, PO Box 392, Pretoria-South Africa.*

PbS thin films were deposited on glass and stainless steel substrates using PACBD method. The as-deposited and annealed films were characterized for structural, morphological, compositional, optical and electrochemical properties. Cyclic voltammetry indicated a reversible redox reaction with electrochemical interfacial capacitance of 101mF/cm^2 and 75mF/cm^2 for as-deposited and 200^{o}C-annealed films repectively at 20mV/s scan rate. Phase angle of impedance was less negative than that of a perfect capacitor (-90), indicating frequency dispersion. Constant phase element was used to fit interfacial capacitance in the corresponding equivalent circuit. Incoporation of PVP into PbS matrix enhanced its electrochemical properties compared to typical PbS film.

(Received November 9, 2014; Accepted January 12, 2015)

Keywords: Cyclic voltammetry; PbS; Polymer-assisted-chemical-bath-deposition; PVP; Thin film

1. Introduction

Semiconductor materials are increasingly generating interest due to their outstanding electronic and optical properties and potential applications in various devices. The electronic and optical properties of semiconductor materials could be altered by varying their sizes and shapes [1]. Therefore, the optimization of synthesis parameters of these nano-particles is important in order to improve their properties. The fabrication technique of nanoscale materials with controlled shape and high dispersion using polymeric or other conventional capping materials is known as capping-assisted chemical bath deposition (CACBD) technique. As an important IV-VI group semiconductor, lead sulphide is a direct narrow band gap semiconductor material of ≈ 0.41 eV at room temperature [2] and has a relatively large excitation Bohr radius of 18 nm [3] making it an interesting material to study the quantum effects over the wide range of particle size [4]. Quantum size effects are usually characteristic of nanocrystallites measuring less than 10 nm. This property makes it an excellent candidate for opto-electronic applications in many fields such as photography, IR detectors, solar absorbers, light emitting devices and solar cells [5, 6, 7, 8, and 9].

*Corresponding author: fiezema@yahoo.com

Hence, there has been growing interest in developing techniques for preparing semiconductor nano-particle films. These materials can be obtained in thin film form by various methods, including chemical bath deposition [10], electrodeposition [11], and microwave heating [12]. The chemical bath deposition (CBD) is simple, economical and convenient for large area deposition of IV-VI compounds [13].

The use of polymer protection like polyvinyl pyrrolidone (PVP) has been found to regulate the pattern of arrangement of particles. Zongtao *et al* [14] have reported a PVP protective mechanism of ultrafine silver powder synthesized by chemical reduction processes in which PVP as a protective agent plays a decisive part in controlling superfine silver particle size and size distribution by reducing silver nitrate with hydrazine hydrate. Using a newly developed chemical method, known as the polymer protected reduction process, Fievet *et al.* [15] and Ducamp-Sanguesa *et al.* [16], employed PVP as a protective agent to synthesize ultrafine silver powder with 300 nm diameter, by reducing silver nitrate with hot polyol solution. Tosun and Glichsman [17] have also reported a gelatin protected processing, which was similar to that of PVP.

Numerous inorganic and organic polymer composite nano-fibers have been prepared by electrospinning method. Wang and co-workers [18-21] have successfully formed composite nano-fibers of metal sulfide nano-particles and polymer nano-fibers, such as PbS/poly(vinyl pyrrolidone), CdS/PVP, Ag_2S/PVP and Ag_2S/polyacrylonitrile (PAN). In their studies, the metal salt/polymer nano-fibers were obtained via electrospinning method, and then the metal nano-particles were formed in the nano-fibers via gas–solid reaction of metal ion and gaseous H_2S.

Given the wide range of present and future possible applications of PbS, various methods have been used to study its physical and semiconducting properties. Electrochemical studies of semiconductors such as PbS have the advantage that charge transfer can be registered and characterized in terms of their peak potentials and current intensity. Studies have also shown that there is a correlation between optical band gaps obtained from absorption measurements and the difference between the oxidation and reduction peaks potentials from cyclic voltammetry [22, 23]. Electrochemical Impedance Spectroscopy (EIS) is a widely used technique to investigate the properties of semiconductor electrodes in an electrolyte solution. The advantage of EIS is that it is generally non-destructive to the investigated system and has the potential to provide information about the physical and electrical properties of semiconducting materials. Accurate results are obtained by fitting the impedance data to an appropriate equivalent circuit (EC) which consists mainly of common electric elements, such as resistors, capacitors and inductors. Electrochemical methods have been used by some authors to investigate the properties of both quantum dot PbS and thin film PbS deposited by various methods [24-27]. To the best of the knowledge of the authors, the electrochemical properties of PbS films incorporated with PVP have not been studied.

In this work, we study for the first time; the electrochemical behavior of PVP capped PbS thin films deposited by CBD. The aim of the study is to probe the electrochemical response of the PVP capped PbS in 1M NaOH solution using cyclic voltammetry, galvanostatic charge-discharge and electrochemical impedance spectroscopy. The influence of the PVP incorporation into the matrix of the PbS film and the effect of annealing on its properties are also presented. The results provide a useful understanding of the processes at the PbS/electrolyte interface. The structural, morphological and optical properties of nanocrystalline PbS/PVP- based nanocrystalline films were obtained using, X-Ray diffraction, scanning electron microscope and UV-Vis-NIR spectrophotometer respectively.

2. Experimental

All the chemicals used for the deposition were analytical grade and all the solutions were prepared in distilled water. Stainless steel and glass were used as substrates. The steel substrates were polished with zero grade emery polish papers washed with plenty of water and detergent, ultrasonicated in a mixture of acetone and distilled water, rinsed in distilled water and then dried. The glass substrates were suitably cleaned in detergent, sulphuric acid and distilled water, rinsed in ethanol, acetone, and distilled water and dried in an oven. The bath for the thin films were then prepared using 0.05 M Lead acetate ($Pb(CH_3OO)_2$) solution, 0.10 M Thiourea ($(NH_2)_2SC$), 1.00M

sodium hydroxide (NaOH) and poly(vinyl pyrrolidone) $(C_6H_9NO)n$ as the starting precursors. The pH of the resulting solution was adjusted to 11 with the NaOH. The previously prepared substrates were vertically suspended in the beaker. The deposition was achieved after 45 min at 27^{o}C. Subsequently, the substrates were taken out of the bath, rinsed with distilled water, dried and preserved in a dust-free container. Some of the samples of the PbS thin films were annealed at 100^{o}C, 200 ^{o}C, 300 ^{o}C and 400 ^{o}C while others are left as deposited.

X-ray diffraction studies were carried out on all the samples using X'Pert HighScore PW1710 PANanalytical diffractometer in the scanning range of 2θ from $10^o - 60^o$ with Cu-kα (λ = 1.5406 Å) radiations. The surface morphology and composition studies were carried out using scanning electron microscopy (SEM) and energy dispersive analysis by X-ray (EDAX) (JEOL-JSM 5600, Japan). The optical absorption studies were carried out using UV-VIS-NIR spectrophotometer (Unico- UV- 2102PC, Japan) in the 200-1000 nm wavelength range. The electrochemical properties of the films were determined using a three-electrode system connected to a potentiostat (Princeton Applied Research VersaSTAT). The working electrode is PVP/PbS on stainless steel polished with zero grade emery papers while the counter electrode is graphite rod. Ag/AgCl/KCl (sat.) was used as a reference electrode and all the potentials cited in the present study are referred to this electrode unless otherwise stated.

3. Results and discussion

3.1 Thin film formation process of the PVP capped PbS films

The possible reaction process synthesis of PVP capped PbS thin films in solution is:

$$Pb(CH_3COO)_2 + 2NaOH \rightarrow Pb(OH)_2 + 2Na(CH_3COO) \quad (1)$$

$$Pb(OH)_2 + 4NaOH \rightarrow 4Na^+ + HPbO_2^- + 3OH^- + H_2O \quad (2)$$

In alkaline medium, thiourea decomposes and releases S^{2-} ions, which precipitates Pb^{2+} ions from solution.

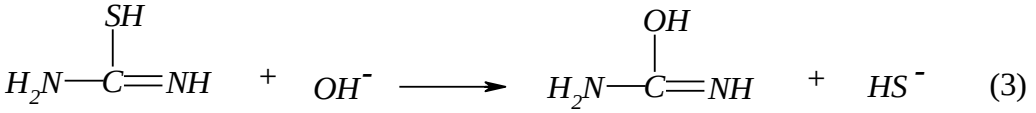

(3)

$$HPbO_2^- + HS^- \rightarrow PbS + 2OH^- \quad (4)$$

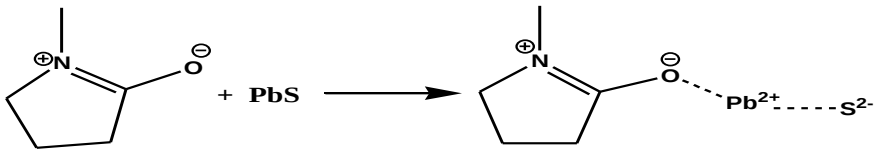

(5)

Deposition of the films from a solution involves a nucleation phase in which an initial layer of $Pb(OH)_2$, formed on the glass substrate, is chemically converted into PbS by the reaction with S^{2-} ions available in the bath from the hydrolysis of thiourea. The presence of $Pb(OH)_2$ in the as-prepared bath is very vital for the deposition of PbS thin films. PbS then attaches to the PVP. Figure 1 shows a schematic diagram and possible growth mechanism of the PVP-capped PbS thin films and effect of the post thermal treatment on the thin films.

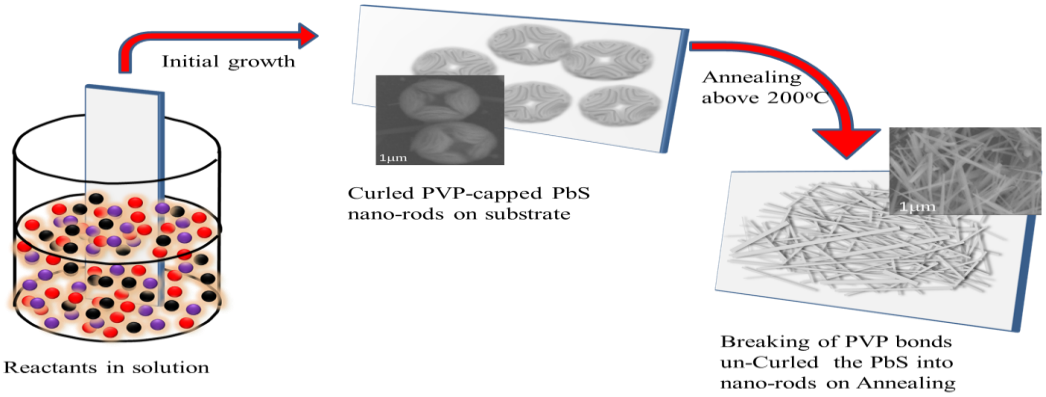

Fig. 1: Growth mechanism of the PVP-capped PbS thin films

The precipitation of metal chalcogenides in CBD occurs only when the ionic product exceeds the solubility product of metal chalcogenides. The film growth takes place via ion-by-ion condensation of the materials or by adsorption of colloidal particles from the solution onto the substrate.

3.2 Structural Analysis

The XRD patterns of the PVP-capped PbS thin films are displayed in Figure 2. The pattern for the as-deposited PVP-capped PbS thin films displayed several diffraction peaks at 2θ values shown in Table 1. The un-annealed sample was amorphous and on annealing, the samples became crystalline. The crystallinity further improved upon annealing the sample at 400^{o}C. There was no significant difference between the peaks of the two annealed samples. However, peaks due to impurities in the sample annealed at 200^{o}C disappeared. The various diffraction 2-theta angles and the corresponding preferred planes of orientation are summarized in Table 1. The XRD patterns compare very well with the standard JCPDS cards (card no. 5-0592). The average grain sizes of the thin films were evaluated using the Scherrer's formula given by

$$D = (k\lambda) / (\beta \cos \Theta) \quad (6)$$

where θ, β, k *and* λ represent the Bragg's angle, the FWHM, a constant (assumed 0.94) and the wavelength of the X-ray (1.54060 Å) respectively. There was an increase in the size of the grains from 7.37 to 10.07nm for thermal treatments at 200^{o}C and 400^{o}C respectively.

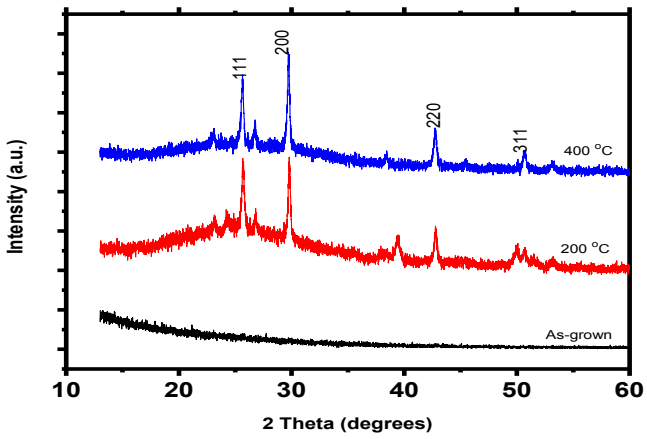

Fig. 2. The XRD Patterns of the PbS (a) as grown (b) annealed at 200^{o}C (c) annealed at 400^{o}C

Table 1: Summary of the XRD results

Sample	As-deposited	Annealed at 200 ^{o}C	Annealed at 400 ^{o}C
Diffraction peak angles (2θ)	Amorphous	25.71^{o}, 29.79^{o}, 42.76^{o}, 53.25^{o}	25.64^{o}, 29.78^{o}, 42.74^{o}, 53.16^{o}
Diffraction planes (h k l)	-	111, 200, 220, 311	111, 200, 220, 311
Average grain size (nm)	-	7.37	10.07

3.3 Surface morphology and EDAX analysis

Fig. 3 shows the scanning electron micrographs (SEM) of PbS thin films. The SEM of the as-deposited thin films revealed nano-rods which were coiled into flower bud-like or tomato-like structures. These flower-like particles uncurled after being annealed at a temperature of 200^{o}C and above, revealing PbS nano-crystalline rods (1 – 10 μm length). This could possibly be the reason why the XRD of the annealed PbS thin films became more crystalline after the thermal treatment. The size of the PVP-capped PbS nano-rods annealed at 400^{o}C as seen on the SEM confirms the increase in the particle sizes as were calculated using the Scherrer's formula. It was observed that the average rod sizes determined by SEM are comparatively larger than that measured by XRD. The large value of rod sizes may be due to the agglomeration of grains [28], which was widely observed and reported by various authors [29- 31]. This suggests that the PbS rods are not single crystalline but polycrystalline. It can be inferred that the single crystal sizes measured in the XRD agglomerated to form the nano-rods as seen in the SEM. Comparatively, Wang and co-workers [18] reported PbS nano-particles dispersed in polymer-fiber matrices by electrospinning obtained PbS nano-particles roughly spherical in shape, each with a diameter of approximately 5 nm, and did not aggregate. Shi et al [32] reported a great change in morphologies of products with varying PVP amounts revealing that the PVP-assisted dynamical crystal growth process was responsible for the formation of BiOBr HNs and speculated that PVP can regulate the morphology of samples and control the thickness and distance of nano-sheets. This work agrees with that speculation that PVP is responsible for the shape gotten in the as-grown and was destroyed by heat during the annealing process. On annealing, there is a transformation to crystalline state, since PVP has a melting point of 150-180^{o}C (glass temperature). This possibly suggests that PVP here serves as a medium to assemble the nano-particles and also stabilize them against aggregation.

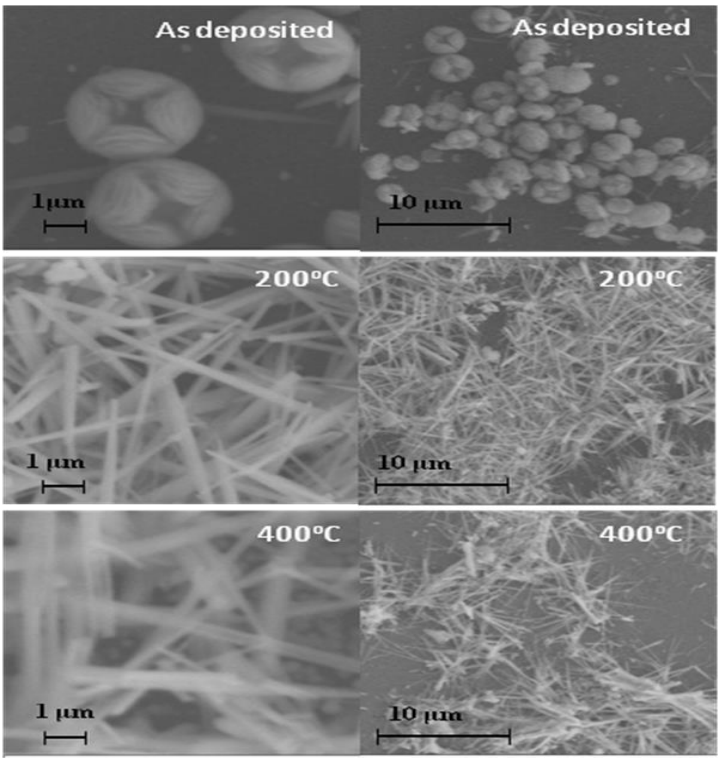

Fig. 3: SEM micrograph of the PbS (a) as grown (b) annealed at 200°C (c) annealed at 400°C

The energy-dispersive analysis by X-ray was used to determine the composition of PbS thin film as shown in figure 4. The elemental ratios of Pb:S calculated from the spectra were ≈ 1:1, 1:1 and 4:1 for as-deposited, annealed at 200°C and 400°C respectively. It appeared that sulphur was slightly higher than lead for as-deposited, exactly equal for sample annealed at 200°C and significantly less than lead for sample annealed at 400°C. It can be inferred that the sulphur was vaporizing with increase in temperature. This confirmed that the films were rich in lead (Pb). Other elements seen as components of the glass substrate were: Si, Na, K, Ca, Al, Mg and O.

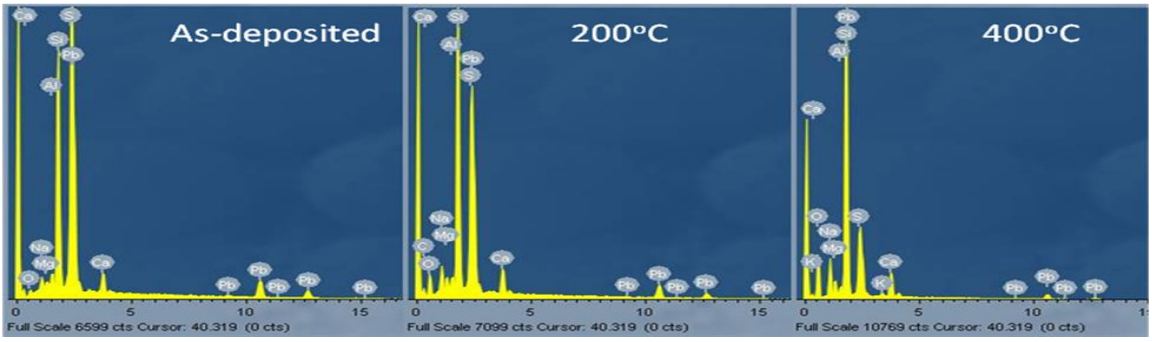

Fig. 4: EDAX plot for PVP-capped PbS thin film (a) as grown (b) annealed at 200°C (c) annealed at 400°C

3.4 Optical studies

All the samples had very low transmittance in the visible region but higher towards the near infra red region. This increased from as low as 5% in the VIS region to about 40% at the NIR region of the electromagnetic spectrum as can be seen in Figure 5. Though there is no trend, Figure 5 shows that transmittance decreased with increase in annealing temperature. This may be due to

scattering and absorption of light, since after annealing, films become denser and for denser films, scattering and absorption of light is higher.

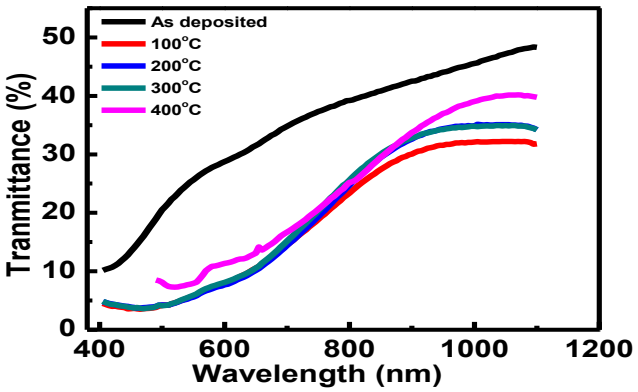

Fig. 5. Plot of transmittance Vs wavelength of the photons (a) as grown (b)annealed at 100°C (c) annealed at 200°C (d) annealed at 300°C (e) annealed at 400°C

The band gap energy (E_g) of the deposited films was obtained by analyzing the optical data using the expression:

$$\alpha h\nu = C\,(h\nu - E_g)^n \tag{7}$$

where α is optical absorbance, $h\nu$ is photon energy, C is a constant and the exponential n depends on the type of transition. Figure 6 is a plot of $(\alpha h\nu)^2$ versus photon energy ($h\nu$) of PbS thin films. The energy gaps for these films are obtained by extrapolating the linear part of the curve to the energy axis. PbS thin film exhibits direct band transition, the band gap energy obtained for the thin films are 2.25 eV, 1.55 eV, 1.55 eV, 1.58 eV, 1.48 eV for the as-deposited,100°C, 200°C, 300°C, 400°C respectively as estimated from figure 6. The values of the band gap were higher than that of bulk PbS (0.41eV), the blue shift from the near IR to the visible region is 1.84 eV, 1.14 eV, 1.14 eV, 1.17 eV, and 1.07 eV for the as-deposited, 100°C, 200°C, 300°C, 400°C respectively. The band gap decreases with increase in annealing temperature which implies that better quantum confinement takes place at higher annealing temperature, thereby, exhibiting good optical properties.

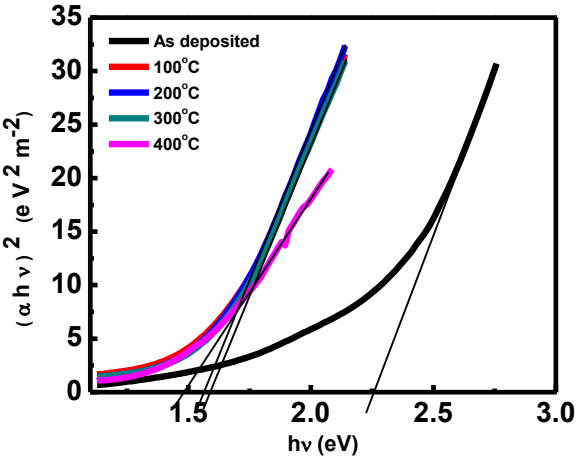

Fig. 6: Plot of $(ahv)^2$ as a function of photon energy (hv) for the Lead sulfide thin films (a) as grown (b)annealed at 100°C (c) annealed at 200°C (d) annealed at 300°C (e) annealed at 400°C

3.5 Electrochemical Properties of PbS

3.5.1 Cyclic Voltammetry

Fig. 7 (*a* and *b*) gives the cyclic voltammetry (CV) of the as-deposited and annealed films (200^{o}C) respectively on the stainless steel (ss) and recorded in 1M NaOH solution in a potential window of -0.8 to +0.8V vs Ag/AgCl/KCl (sat) at different scan rates. During the anodic scan, two prominent peaks are observed at A1 and A2. It is noticed that at higher currents, peaks at A1 become more defined while the peaks at A2 shifts anodically. The anodic peaks observed are due to the oxidation of PbS while the anodic shift of the formal potential is due to reduction in the pH as the CV current increased [24].

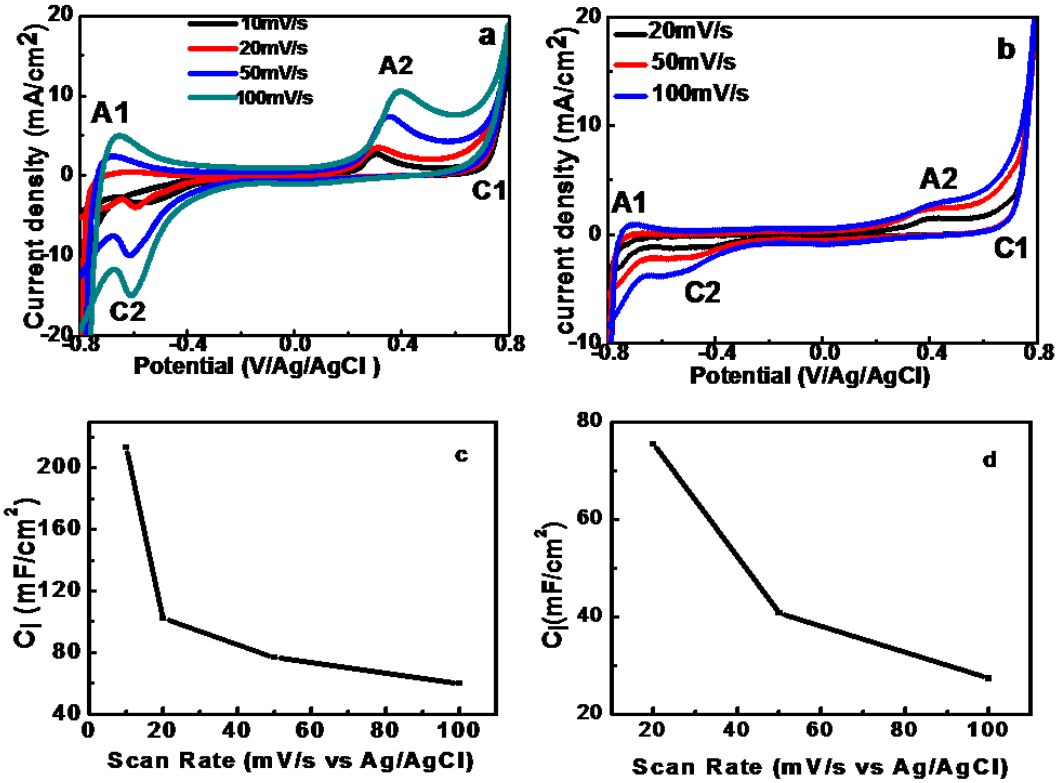

Fig. 7: Cyclic Voltammetry of the (a) un-annealed film, (b) 200^{o}C annealed film; interfacial capacitance Vs Scan rate for (c) un-annealed film, (d) 200^{o}C annealed film

The oxidation reaction of PbS has been found to be pH dependent, with lower pH favoring the passivation of the PbS surface due to the formation of crystalline sulphur [25]. High pH values of the electrolyte favour the formation of plumbite and sulfate ions along with some S^0 according to the argument of Gardener and Woods [26]. The most thermodynamically favorable oxidation reaction is give as follows:

$$2PbS + 12OH^- - 8e \rightarrow 2HPbO_2^- + S_2O_3^{2+} + 5H_2O \quad (8)$$

Some of the PbS may dissolve during oxidation and diffuse into the bulk of the electrolyte solution. It has been shown that this PbS restores from adsorbed species at potentials <~ –0.6 V but not from those surrounding the electrode [24]. The CV exhibits two cathodic peaks C_1 and C_2 due to the reduction of the plumbite and sulfate ions. Each of the CV curve consists of a pair of redox peaks A_1C_1 and A_2C_2 indicating the reversibility of the process hence equation above can be written as as redox equation.

$$2PbS + 12OH^- - 8e \Leftrightarrow 2HPbO_2^- + S_2O_3^{2+} + 5H_2O \quad (9)$$

This reversibility is not observed in most of the studied cyclic voltammetry of PbS [24-27] and may have been enhanced by the incorporation of PVP in the PbS matrix.

Based on the observed reversibility, the electrochemical capacitive properties of the films were investigated. The linear increase in both the anodic and cathodic peak potential as the scan rate increases indicates that the redox mechanism is diffusion controlled. This increase is less for the annealed film compared with the un-annealed film. This confirms that the PVP plays a very significant role in the electrochemical properties of PbS film because it has been shown that during the heat treatment, the PVP that formed as a passivation layer around the PbS breaks down producing shorter polymer chains that open up the encapsulation of PVP on the surface of the metallic ions [27]. The CV curves show sharp redox peaks indicating that the electrochemical capacitance is due mainly to redox reactions rather than electric double layer capacitance.

The interfacial capacitance of the PbS films was calculated from the CV curves using equations 10:

$$C_i = \frac{\int Idt}{A(dV/dt)} \quad (10)$$

Where C_i is the specific capacitance (F/cm), $\int Idt$ is the area under the CVcurve, A is the area of the electrode dipped in the electrolyte (cm) and dV/dt is the scan rate (mV/s). The graph of the interfacial capacitance as function of the scan rate is shown in figure 7 (c and d) for the unannealed and 200^{o}C annealed films respectively. The value of C_i equals 101mF/cm^2 and 75mF/cm^2 for the unannealed and annealed films repectively at a scan rate of 20mV/s. The reduced C_i for the annealed film could also be attributed to the breakdown of the PVP. It is observed that the specific capacitance decreased with increased scan rates. This may be due to the inability of inner active sites at an electrode surface to carry out redox transitions with increase in scan rates [33].

3.5.2. Galvanostatic charge-discharge (GCD)

GCD test were carried out on the films in a three-electrode system with 1M NaOH at various current densities. The shape of the discharge as shown in figure 8 contains two parts; a linear part due to voltage drop across the equivalent series resisitance (ESR) and a non linear part due to faradaic reactions at the electrode surface contributing to the charge storage. This behavior suggests the pseudocapacitive bahavior of the electrodes. Comparing the GCD of the as deposited and the annealed film at 1mA/cm^2, it is observed that the unannealed had a longer discharge time than the annealed. This could also be attributed to the breakdown of the PVP at higher temperature. The specific energy, specific power and columbic efficiency was calculated at a current density of 1mA/cm^2 with respect to the area of deposit using the following equations:

$$SE = \frac{V \times I_d \times T_d}{A} \quad (11)$$

$$SP = \frac{V \times I_d}{A} \quad (12)$$

$$Coulombic\ efficiency\ \eta(\%) = \frac{T_d}{T_c} \times 100 \quad (13)$$

where *SE* and *SP* is the specific energy and specific power respectively, V is the voltage range, I_d and T_d is the discharge current and discharge time respectively, *A* is the electrode area with the deposit, T_c is the charging time. The calculated *SE* is 23.4 μWh/cm^2 and 21.8 μWh/cm^2 while *SP* is

3 mW/cm^2 and 2.8 mW/cm^2 respectively for the as deposited and annealed film. The coulombic efficiency obtained is 95 % for the as deposited and 100 % for the annealed film.

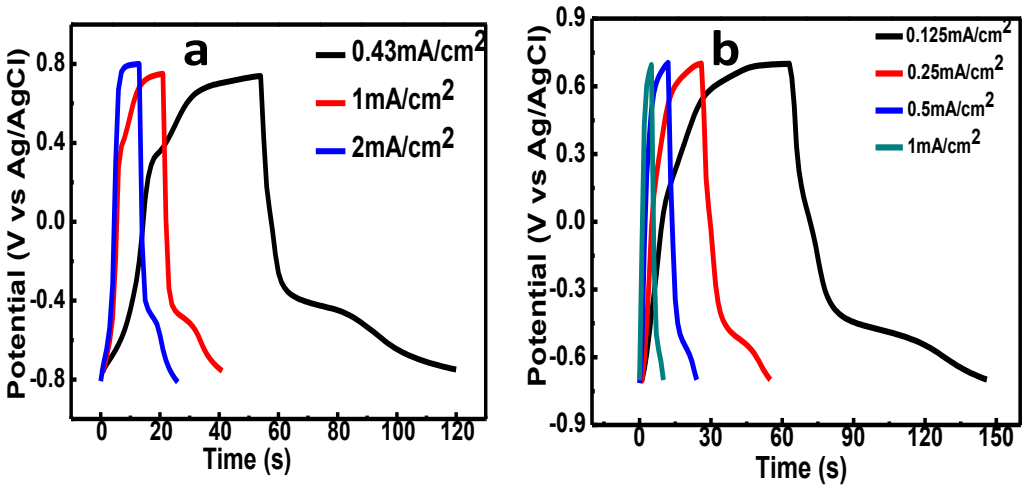

Fig. 8: Galvanostatic charge discharge curve for the films (a) as deposited (b) annealed at 200^{o}C

3.5.3. Electrochemical Impedance Spectroscopy.

The Nyquist plot for the PVP-capped PbS films recorded using a three electrode system in 1M NaOH electrolyte and at a freqency range of 0.01H-100kH with an ac amplitude of 10mV is shown in figure 9*a*.

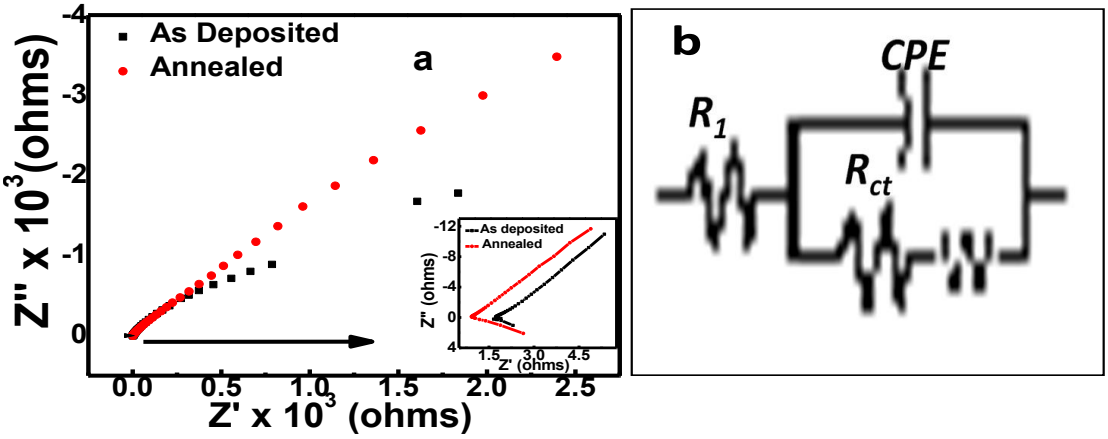

Fig. 9: (a) Nyquist plot, (b) Equivalent circuit diagram

The Nyquist diagrams exhibit depressed capacitive semi-circle in high frequency region as shown in the inset. The extent of depression of the semi-circle in the Nyquist plots signifies the non-ideal contacts, etc. exemplified as CPEs instead of ideal capacitors in the equivalent circuit [27]. The equivalent circuit and the fitted values of the circuit parametres were obtained using ZSimpWin software and is shown in figure 9b and table 2 respectively. In the electrical equivalent circuit, R_s, R_{ct} and *CPE* represent the electrolyte solution resistance, the charge transfer resistance at the electrode/electrolyte interface and a constant phase element corresponding to space charge capacitance respectively. Other phenomena such as dynamic disorder associated with diffusion, dielectric relaxation either in the space charge layer or at the semiconductor-electrolyte interface, surface states and roughness of electrode surface [34-37] have been used to explain the CPE behavior on the semiconductor electrodes. The Warburg (W) gives an indication of the ion

diffusion into the electrode materials and is seen in the intermediate frequency at the 45^o line to the imaginary impedance (Z") axis.

Table 2: Fitted circuit parameters for the equivalent circuit.

Circuit Elements	**As-deposited**	**200^{o}C annealed film**
R_s (Ω)	2.067	1.55
CPE1 (F)	0.000351	0.0003261
R_{ct}(Ω)	0.7472	0.1296
W(S-sec^0.5)	0.001082	0.001178

The plot of /Z/ against frequency from the Bode plot (figure 10) shows an increase in impedance toward the low frequencies and impedance relaxation toward the high frequencies. It is also seen that the phase angle of the impedance is less negative than that of a perfect capacitor (-90), indicating frequency dispersion. The Bode plot and the fitted result for the as deposited and the annealed sample at 200^{o}C is shown in figure 11. The figures show a good agreement between the experimental and impedance fitted data.

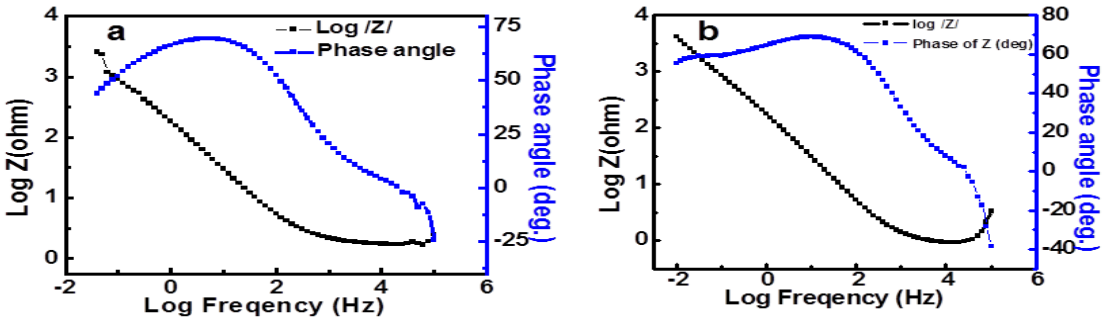

Fig. 10: Bode plot for (a) As deposited film (b) 200^{o}C annealed film

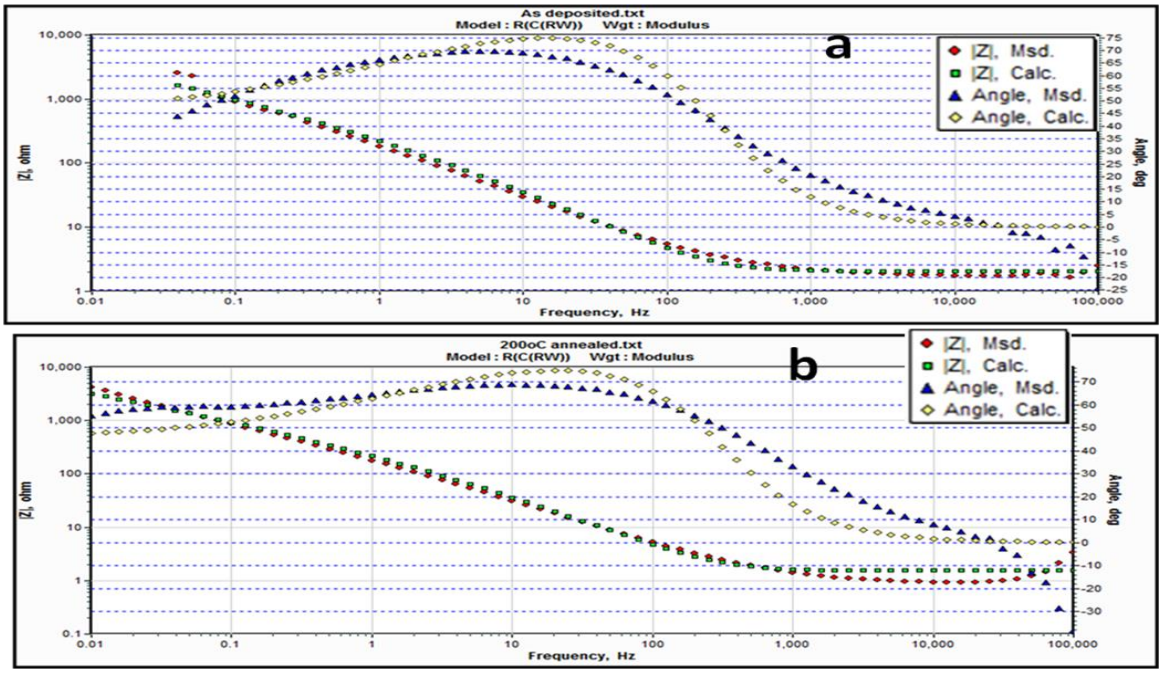

Fig. 11: Bode plot of experimental and fitted data for the (a) as deposit film (b) annealed film at 200^{o}C

4. Conclusion

We successfully deposited PbS thin films on stainless steel and glass substrates using PVP as the deposition medium. Thermal treatments improved the crystallinity of the PVP-capped PbS thin films and the average grain sizes were between 7.37 and 10.07nm as calculated from XRD. The SEM of the thin films revealed nano-crystalline rods of length between 1.0 and 10.0 μm which consisted of agglomeration of the grains. The incorporation of PVP into the PbS films enhanced its electrochemical properties giving a reversibility in the redox reactions that is not peculiar with other studied PbS films. The interfacial electrochemical capacitance calculated from the CV curves is 101mF/cm^2 and 75mF/cm^2 for the unannealed and 200^{o}C annealed films respectively at a scan rate of 20mV/s. We can autoritatively say that the PVP-capped PbS films gave electrochemical properties that is suitable for application as an electrode in supercapacitors.

References

[1] P. D. Yang, C. M. Lieber, Sci., **273**, 1836 (1996).
[2] S. Seghaier, N. Kamoun, R. Brini, A. B. Amara, Mater. Chem. Phys., **97**, 71 (2006).
[3] J.L. Machol, F.W. Wise, R.C. Patel, D.B. Tanner, Phys. Rev. B., **48**, 2819 (1993).
[4] J. E. Murphy, M. C. Beard, A. G. Norman, S. P. Ahrenkiel, J. C. Johnson, P. Yu, O. I. Micic, R. J. Ellingson, A. J. Nozik, J. Am. Chem. Soc., **128**, 3241 (2006).
[5] P. K. Nair, O. Gomezdaza, M. T. S. Nair, Adv. Mater. Opt. Electron., **1**, 139 (1992).
[6] P. Gadenne, Y. Yagil, G. Deutscher, J. Appl. Phys., **66**, 3019 (1989).
[7] T. K. Chaudhuri, S. Chatterjee, *Proc. of 11th Int. Conf. Thermoelectrics*, Arlington, USA 40 (1992).
[8] S. A. Mcdonald, G. Konstantatos, S. Zhang, P. W. Cyr, E. J. D. Klem, L. Levina, E. H. Sargent, Nat. Mater., **4**, 138 (2005).
[9] E. H. Sargent, Adv. Mater., **17**, 515 (2005).
[10] G. Schmidt, Chem. Rev., **92**, 1709 (1992).
[11] A.N. Molin, A.I. Dikusar, Thin Solid Films **265**, 3 (1995).
[12] J. J. Zhu, O. Palchik, S.G. Chem, A. Gedanken, J. Phys. Chem., **104**, 7344 (2000).
[13] M. A. Barote, B. D. Ingale, R. V. Suryawanshi, T. V. Chavan, E. U Masumdar, Res .J. Chem. Sci., **1**(5), 48 (2011).
[14] Zongtao Zhang, Bin Zhao, Liming Hu. J. of Solid State Chem., **121**, 105 (1996).
[15] F. Fievet, J. P. Lagier, B. Blin, Solid State Ionics**, 32/33**, 198 (1989). In: Zongtao Zhang, Bin Zhao, and Liming Hu. J. of Solid State Chem., **121**, 105 (1996).
[16] C. Ducamp-Sanguesa, R. Herrera-Orbina, M. Figlarz, J. Solid State Chem., **100,** 272 (1992). In: Zongtao Zhang, Bin Zhao, and Liming Hu. J. of Solid State Chem., **121**, 105 (1996).
[17] G. Tosun, H.D. Glicjsman, U.S. Patent 4,978,985. In: Zongtao Zhang, Bin Zhao, Liming Hu, J. of Solid State Chem., **121**, 105 (1996).
[18] X. Lu, Y. Zhao, C.Wang, Adv. Mater., **17**, 2485 (2005).
[19] X.F. Lu, Y.Y. Zhao, C.Wang, Y.Wei, Macromol. Rapid Commun., **26**, 1325 (2005). In: Jie Bai, Yaoxian Li, Chaoqun Zhang, Xiaofei Liang, Qingbiao Yang, Colloids and Surf. A., **329**, 165 (2008).
[20] X.F. Lu, L.L. Li, W.J. Zhang, C.Wang, Nanotech., **16**, 2233 (2005). In: Jie Bai, Yaoxian Li, Chaoqun Zhang, Xiaofei Liang, Qingbiao Yang, Colloids and Surf. A., **329**, 165 (2008).
[21] F.X. Dong, Z.Y. Li, H.M. Huang, F. Yang,W. Zheng, C.Wang, Mater. Lett., **61**, 2556 (2007).
[22] S.N. Inamdar, P.P. Ingole, S.K. Haram, Chem. Phys. Chem., **9(**17), 2574 (2008).
[23] D.M.N.M. Dissanayake, T. Lutz, R.J. Curry, S.R.P. Silva, Appl. Phys. Lett. **93**, no. 043501 (2008).
[24] A. S. Cuharuc, L. L. Kulyuk, R. I. Lascova, A. A. Mitioglu, and A. I. Dikusar, Surf. Eng. and Appl. Electrochem., **48(**3), 193 (2012).
[25] Yu. Mikhlin, A. Kuklinskiy, E. Mikhlina, V. Kargin, I. Asanov, J. Appl. Electrochem., **34**, 37 (2004).
[26] J.R. Gardener, and R. Woods, J. Electroanal. Chem., **100(**1–2), 447 (1979).

[27] A. Aghassi, M. Jafarian, I. Danaee, F. Gobal, M.G. Mahjani, J. Electroanal. Chem., **661**, 265 (2011).
[28] S. Chowdhury, S. K. Dolui, D. K. Avasthi & A. Choudhury, Indian J Phys. & Proc. Indian Assoc. Cultivation Sci-New Series. **79**, 1019 (2005).
[29] M.A. Barote, A.A. Yadav, T.V. Chavan, E.U. Masumdar, J. Nanomat. and Biostruc., **6**, 979 (2011).
[30] J.D. Patel, F. Mighri, A. Ajji, T.K. Chaudhuri, Mat. Chem. and Phys., **132**, 747 (2012).
[31] N. Soltani, E. Saion, M. Erfani, K. Rezaee, G. Bahmanrokh, G.P.C. Drummen, A. Bahrami, M.Z. Husseni, Int. J. Mol. Sci., **13**, 12412 (2012).
[32] Xiaojing Shi, Xin Chen, Xiliang Chen, Shaomin Zhou, Shiyun Lou, Yongqiang Wang, Lin Yuan, Chem. Eng. J., **222**, 120 (2013).
[33] V. S. Kumbhar, A.D. Jagadale, N. M. Shinde, C. D. Lokhande, Appl. Surf. Sci., **259**, 39 (2012).
[34] D.P. Dubal, S. H. Lee, J. G. Kim, W. B. Kim, C.D. Lokhande, J. Mat. Chem.**,** **22**, 3044 (2012).
[35] A. Goossens, J. Schoonman, J. Electrochem. Soc., **139**, 893 (1992).
[36] E.C. Dutoit, R.L. Van Meirhaeghe, F. Cardon, W.P. Gomes, Ber. Bunsenges. Phys. Chem., **79**, 1206 (1975).
[37] G. Oskam, D. Vanmaekelbergh, J.J. Kelly, J. Electroanal. Chem., **315**, 65 (1991).